RSC Advances

PAPER

View Article Online
View Journal | View Issue

Cite this: *RSC Adv.*, 2019, **9**, 8490

First-principles study of the effect of dopants (Pd, Ni) on the formation and desorption of T_2O from a Li_2TiO_3 (001) surface

Yiyu Fang,[a] Xianggang Kong,[b] You Yu,[b] Xiaotong Zhang,[a] Xiaojun Chen,[c] Tao Gao,*[ad] Chengjian Xiao*[c] and Tiecheng Lu[d]

Received 31st January 2019
Accepted 7th March 2019

DOI: 10.1039/c9ra00830f

rsc.li/rsc-advances

We investigated the effect of Pd and Ni dopants on the formation and desorption of tritiated water (T_2O) molecules from the Li_2TiO_3 (001) surface using first-principles calculations coupled with the climbing-image nudged elastic band method. We calculated the energy barriers for T_2O production and desorption on the pure Li_2TiO_3 surface to be 0.94 and 0.64 eV, respectively. The Pd and Ni dopants enhanced T_2O formation by reducing the formation energy of O vacancies, and T_2O generated spontaneously on the dopant surface. Moreover, we found that dopant atoms affect the charge transfer of neighboring atoms, which leads to orbital hybridization and the generation of a chemical bond between the O and T on the doped Li_2TiO_3 surface. In addition, desorption of T_2O from the doped Li_2TiO_3 surface requires a relatively low energy (<0.50 eV). This theoretical study suggests that doping the Li_2TiO_3 surface with metal atoms is an effective strategy for producing T_2O molecules and is beneficial to T release.

1. Introduction

Tritium breeding blankets and energy extraction are crucial for the development of deuterium–tritium (D–T) nuclear fusion power reactors. Most designs of D–T fusion reactor blankets use solid lithium ceramics as the breeder material because it is thermodynamically, chemically and mechanically stable, has a high lithium density and melting point, and excellent tritium release properties. Consequently, breeder blankets based on lithium ceramics can withstand high temperatures and extended periods of radiation at high temperature gradients.[1–3]

Compounds such as Li_2O, $LiAlO_2$, Li_4SiO_4, Li_2SiO_3, Li_2ZrO_3, Li_2SnO_3, and Li_2TiO_3 (ref. 4–10) are considered to be the most favorable candidates for breeding blankets. For example, in the helium-cooled solid pebble beds (HCSPB) design of the International Thermonuclear Experimental Reactor (ITER), Li_2TiO_3 is used.[11,12] Experimental studies have revealed the detailed mechanisms of the tritium generated after the nuclear reaction. Li_2TiO_3 has excellent performance at in low activity, such that the neutrons can penetrate the Li_2TiO_3 matrix easily. The tritium must then diffuse to the pebble surface, where it transfers to a surface water layer before undergoing isotope exchange. And tritium will be adsorbed on the surface of the lithium ceramic forming hydroxyl groups.[11,13] The amount of tritium retained in Li_2TiO_3 is the lowest in the crystal particles, and the tritium mainly remains in the surface layer and the interface layer of the crystal particles.[14] Moreover, the desorption of tritium from the ceramic surface is the rate-determining step in the tritium extraction process. Ineffective tritium release and collection affects the supply of raw materials for the fusion reaction, and leads to structural change and volume expansion of the ceramic.[15]

The tritium release behavior of Li_2TiO_3 ceramics has been widely investigated. It was found that the release rate is improved at temperatures above 873 K.[11] Moreover, when a palladium is deposited on the surface of Li_2TiO_3 or Li_4SiO_4, it is likely to promote the isotope exchange reaction on the surface of the breeder, improving the release efficiency of tritium will be greatly improved at low temperature.[16] In another study, dopant atoms, such as Pt, Pd and Ni, in the surface of lithium silicate material were also shown to improve the release efficiency of tritium.[17,18] In addition, doping of Mg or Pt in $LiAlO_2$, the release of tritium at low temperature by reducing the desorption activation energy of tritium on the surface.[19] Furthermore, it was found that the effect of the catalyst on the isotopic exchange reaction of Li_2TiO_3 was more pronounced than that of Li_4SiO_4.[16] In light of these experimental observations, it is vital to conduct theoretical studies on the effect of metal impurities on the Li_2TiO_3 surface.

Few theoretical investigations have been reported about the release behavior of tritium from the Li_2TiO_3 surface. Therefore, the aim of this work was to determine the release behavior of

[a]*Institute of Atomic and Molecular Physics, Sichuan University, Chengdu 610065, People's Republic of China. E-mail: gaotao@scu.edu.cn*

[b]*College of Optoelectronic Technology, Chengdu University of Information Technology, Chengdu 610225, China*

[c]*Institute of Nuclear Physics and Chemistry, China Academy of Engineering Physics, Mianyang 621900, China. E-mail: xiaocj@caep.cn*

[d]*Department of Physics, Key Laboratory for Radiation Physics & Technology of Ministry of Education, Sichuan University, Chengdu 610065, People's Republic of China*

tritium (especially the effect of Pd and Ni) on the surface of a Li_2TiO_3 breeder using density functional theory (DFT). The results of this work may have important implications for the application of Li_2TiO_3 breeders and can also guide future experimental studies into the release of tritium.

2. Theory and methods

All calculations presented herein were carried out with the projector-augmented wave (PAW) formalism of density functional theory (DFT),[20] as implemented in the Vienna *Ab initio* Simulation Package (VASP).[21,22] The generalized gradient approximation (GGA) of Perdew–Burke–Ernzerhof (PBE)[23] was used to calculate the exchange–correlation energy. According to the Born–Oppenheimer approximation, the motion of nuclei and electrons in a molecule can be separated, and systems with T and H atoms have same electronic properties if nuclear motion is not considered. Because this study does not involve vibrational calculations, we used the same properties (*e.g.*, formation energy, desorption energy, local density of state (LDOS), Bader charge, charge density difference (CDD) and other charge properties) for systems with T and H atoms.[24] According to the convergence test, a $3 \times 3 \times 1$ grid of Monkhorst–Pack *K*-point meshes in the Brillouin zone can be used for geometry optimization of the supercell.[25] We set the cut-off energy for plane-wave expansion to 500 eV. The convergence of the total energy is considered to be achieved until two iterated steps with energy difference less than 10^{-5} eV and we considered that the convergence criterion for structural optimization was reached when the maximum force acting on each atom was less than 0.01 eV $Å^{-1}$.

Bader charge analysis, CDD and LDOS were used to analyze the charge transfer. We calculated the energy barriers for the formation and desorption of T_2O on pure Li_2TiO_3 and doped Li_2TiO_3 surfaces using the climbing-image nudged elastic band (CI-NEB) method.[26] In this method, six images were inserted to identify the transition state between the initial state and final state configurations. At low temperature, Li_2TiO_3 crystallizes in the Li_2SnO_3-type β-Li_2TiO_3 structure with the space group C_2/c.[27,28] The unit cell of Li_2TiO_3 is shown in Fig. 1. The equilibrium structure was determined by relaxation with respect to the lattice parameters *a*, *b*, and *c*. The agreement of *a*, *b*, *c* ($a = 5.09$ Å, $b = 8.84$ Å, and $c = 9.67$ Å) with experimental results (see Table 1) was very satisfactory.[27,29]

To determine the most stable surface, we examined the low Miller index surfaces of Li_2TiO_3 by calculating the surface formation energy. The surface energy was calculated according to the following equation:

$$E_{surf} = \frac{E_{slab} - nE_{unit}}{2A} \quad (1)$$

where E_{slab} and E_{unit} are the energies of the relaxed slab system and the unit cell, respectively; *n* is the number of Li_2TiO_3 units; and *A* is the surface area of the slab.

We calculated the (001) plane to be the most thermodynamically stable among the seven low-index surfaces (Table 2), which is consistent with the results of a previous experimental study.[30] When the different atomic termination surfaces (Li-termination slab, Ti-termination slab and O-termination slab) are optimized, the Li-termination slab is the most stable structure, as shown in Table 3. So the Li-termination slab of the surface (001) as the model with $2 \times 1 \times 1$ supercell slab consisting of nine atomic layers. Our convergence tests showed that a single-layer slab is sufficiently thick for our surface model, which contains 96 atoms. The coordinates of the atoms in the upper five layers of the slab are relaxed, while the rest of the atoms in the lower five layers of the slab are constrained at their bulk positions. The theoretical equilibrium lattice parameters of the surface are $a = 10.19$ Å, $b = 8.84$ Å and $c = 24.66$ Å. A vacuum layer of 15 Å was placed along the *z*-direction to eliminate the interaction between periodic surface images in Fig. 1(b).

3. Results and discussions

3.1 Monolayer Li_2TiO_3 doped with Pd/Ni

To explore the catalytic effect of Pd and Ni dopants for the formation of T_2O on the Li_2TiO_3 (001) surface, we studied the structural stability of the doped Li_2TiO_3 system. First, one of the

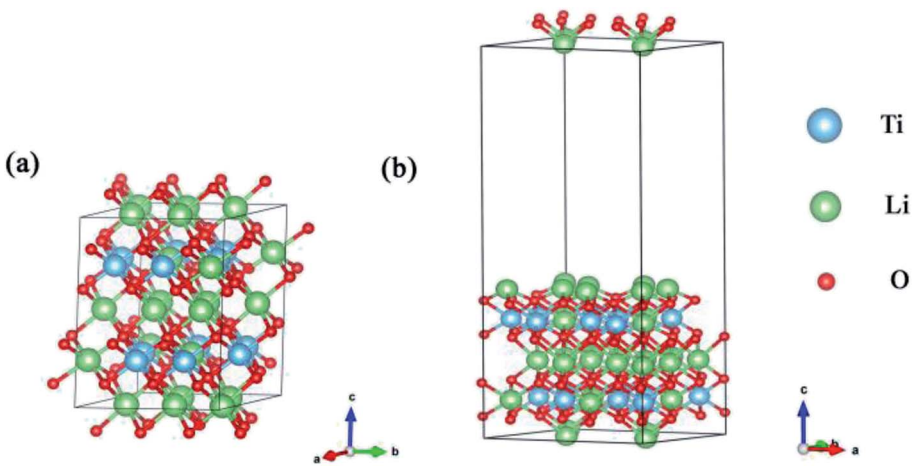

Fig. 1 (a) is the lattice structure of the Li_2TiO_3 unit cell and (b) is the (001) surface. The blue, green and red spheres represent the Ti, Li and O atoms, respectively.

Table 1 Calculated equilibrium lattice parameters of Li_2TiO_3

Parameters	Present	Δ (%)	Experimental[29]	Theoretical[27]
a (Å)	5.0968	0.5%	5.0623(5)	5.0624
b (Å)	8.8464	0.5%	8.7876(9)	8.7877
c (Å)	9.6610	0.8%	9.7533(15)	9.7533

Table 2 The surface energies of low Miller index surface of Li_2TiO_3

Surface	a (Å)	b (Å)	S (Å)	E_c (eV)	E_s (eV)	E_{surf} (eV)
(001)	10.193	8.866	90.381	−336.128	−657.386	0.162
(010)	19.627	5.097	82.256	−336.128	−647.348	0.302
(100)	17.692	9.813	173.632	−336.128	−582.402	0.518
(011)	20.419	11.832	134.372	−336.128	−627.653	0.332
(101)	19.628	10.209	135.589	−336.128	−647.542	0.182
(110)	19.627	10.209	200.372	−336.128	−619.641	0.263
(111)	10.194	13.212	98.086	−336.128	−571.247	1.122

Table 3 Energy of Li-, Ti- or O-termination slabs

Surface	Li-termination	Ti-termination	O-termination
Energy (eV)	−657.392	−511.852	−501.967

Ti atoms was replaced by a Pd or Ni atom in one of two different positions ((1) and (2)) in the third layer[31] as shown in Fig. 2(a and b). This relaxes the surface to a stable state, forming DA-Li_2TiO_3 (the dopant atoms are represented by DA). Then the binding energies (E_b)[32] of the doped surfaces are calculated from the energy difference between the doped Li_2TiO_3 surface (E_P) and the Li_2TiO_3 surface containing the dopant vacancy (E_d):

$$E_b = E_P(Li_2TiO_3) - E_d(Li_2TiO_3; V_{DA}) - \sum_i n_i u_i \quad (2)$$

where n_i is the number of the species added to the surface, u_i is the chemical potential of the dopants. A negative value of E_b indicates an exothermic reaction.

The binding energies calculated for the Pd- and Ni-doped defective monolayer Li_2TiO_3 are listed Table 4 (~−2.80 eV and ~−4.50 eV respectively). All binding energies are negative in the Pd- and Ni-doped systems; that is, these systems are thermodynamically stable.

3.2 Formation and desorption of T_2O on the pure Li_2TiO_3 surface

For comparison with the doped system, we established a model to study the formation and desorption barriers of a T_2O molecule on the pure Li_2TiO_3 surface. Eight Li atoms were replaced by T in the first layer to form the T-Li_2TiO_3 surface to simulate the release process of T_2O, as shown in Fig. 3 and as described in the literature.[33,34]

Fig. 4 presents a pathway with the minimum energy barrier of the formation and desorption of T_2O. The CI-NEB process involves two steps. The first step is the generation of T_2O on the pure Li_2TiO_3 surface. OT attracts the nearest T atoms and results in the production of T_2O on the surface. Next, the T_2O undergoes desorption. The formation and desorption energy barriers were calculated to be 0.94 and 0.64 eV, respectively, which are in good accordance with experimental results observed at annealing temperatures near 500 °C.[16]

3.3 Formation of T_2O on the Pd- and Ni-doped surfaces

Having determined the formation and desorption energies of T_2O on the pure T-Li_2TiO_3 surface (001), we now discuss the results for the Pd- and Ni-doped surfaces. As shown in Fig. 2(c), eight Li atoms are substituted by T in the first layer to study the effect of the dopant atoms (DA) on the release efficiency of

Table 4 Binding energies of the DA-Li_2TiO_3 surface

Dopants	Doped sites	Binding energy (eV)
Pd	Position (1)	−2.70
	Position (2)	−2.81
Ni	Position (1)	−4.51
	Position (2)	−4.54

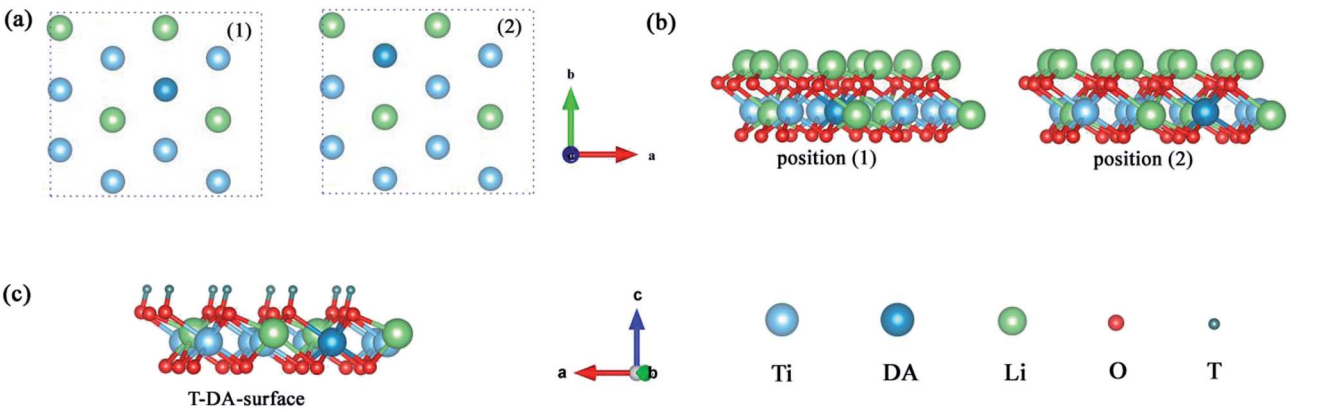

Fig. 2 (a and b) Top and side view representations of DA-Li_2TiO_3 sheets with the metal dopant atoms located in the different positions (using (1) and (2) to represent the positions) in the subsurface. (c) T-DA-surface of the Li_2TiO_3. The red, blue, green, dark green and cyan spheres represent O, Ti, Li, T atoms and DA atoms, respectively.

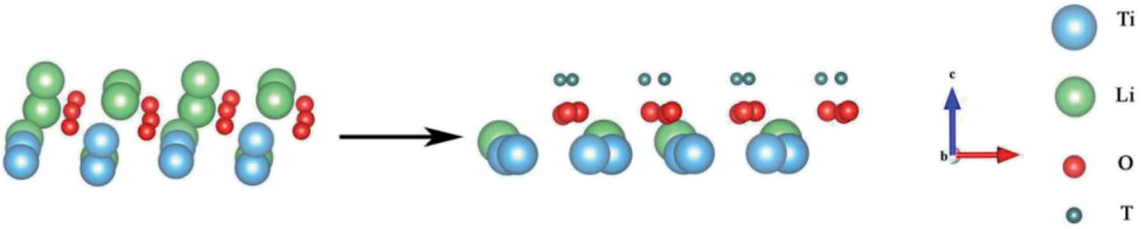

Fig. 3 Li_2TiO_3 and T-Li_2TiO_3 surfaces. The blue, green, red and dark green spheres represent Ti, Li, O and T atoms, respectively.

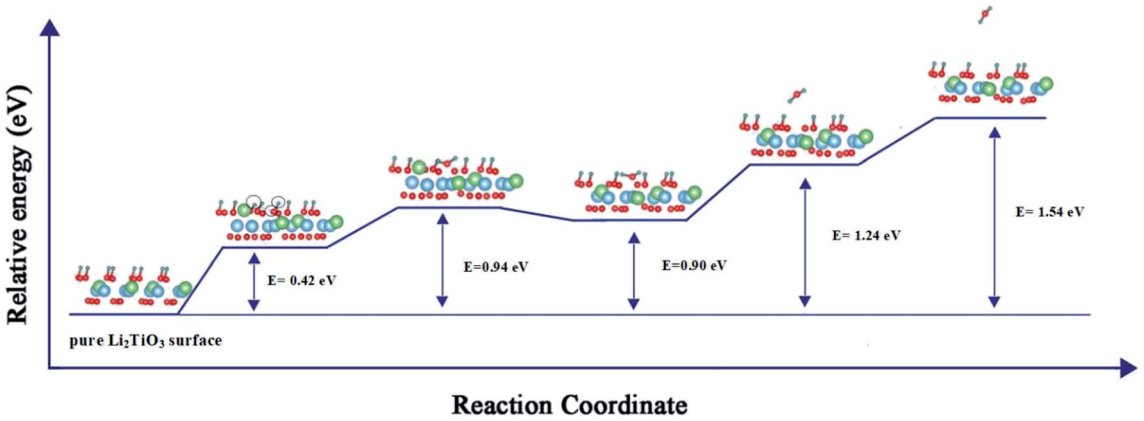

Fig. 4 Formation and desorption energy barriers of T_2O on the T-Li_2TiO_3 surface. The blue, green, red and dark green spheres represent Ti, Li, O and T atoms, respectively. O represents the atom that makes up T_2O.

T_2O.[33] For the T-Li_2TiO_3 surface, there was an energy barrier to T_2O formation in the undoped system. As shown in Fig. 5(a–d), after relaxation of the Pd-/Ni-T-Li_2TiO_3 surface, T_2O molecules spontaneously form on the surface near the DA atom at both at positions (1) and (2). This is in line with experimental results.[16] Comparing with the formation energy of T_2O on the T-Li_2TiO_3 surface, doped atoms can effectively reduce desorption activation energy which are in fair agreement with experimental results that the released capacity of T could be enhanced remarkably on DA-Li_2TiO_3 system. Therefore, Pd, Ni atoms can be seen as the catalyst for the formation of T_2O on the surface of Li_2TiO_3. The calculated formation barrier of T_2 on the surface of pure Li_2TiO_3 is about 1.8 eV, which is higher than that of T_2O (0.94 eV). It is also worth noting that T_2O is produced spontaneously on the surface of DA-Li_2TiO_3, but T_2 is not, indicating that there is still a barrier to T_2 formation in the doped system. We therefore conclude that T_2O is more likely to be produced than T_2 on the surface of Li_2TiO_3, and that metal catalysts (Pd, Ni) have a more pronounced effect on T_2O than T_2. As a result, we focus on T_2O in the next calculation.

To further investigate the catalytic mechanism of the dopants on T_2O formation, we calculated the effect of dopant atoms on the formation energy of O vacancies, according to previous studies.[35,36] The O atoms closest to the dopant atom and the Ti atom substituted on the surface by DA were selected for the study. We define the O vacancy formation energy for Li_2TiO_3 (001) surface as[24]

$$E_{vac} = E(Li_2TiO_3, V_O) + \frac{1}{2}E(O_2) - E(Li_2TiO_3) \quad (3)$$

where $E(Li_2TiO_3, V_O)$, $E(Li_2TiO_3)$ and $E(O_2)$ are the energies of the reduced system, the unreduced surface, and the free O_2 molecule, respectively. Compared with the pure Li_2TiO_3 surface (5.56 eV), the formation energy of O vacancies on the doped surface (~2.75–3.50 eV) are significantly reduced, with O vacancies being more likely to occur, as shown in Table 5. Therefore, the spontaneous generation of T_2O may be caused by the influence of dopant atoms on O vacancies. Intuitively, an easier formation of O vacancies promotes the formation of T_2O.

3.4 The local density of state (LDOS)

In addition to the structural properties, we also studied the electronic properties. Because atoms far from the dopant atoms do not participate in the reaction and just partial atoms of the system take part in the interaction of T_2O formation, the LDOS for the Pd-, Ni-T-Li_2TiO_3 surface is analyzed. Six atoms (the dopant atom; T_1, T_2, and O of the T_2O molecule; Li and Ti) were chosen, and their interactions were investigated on the doped surface. After the formation of T_2O molecules, from the LDOS, the Pd-, and Ni-T-Li_2TiO_3 surfaces have similar electronic structures, with their electronic valence bands moving down (*i.e.*, towards higher binding energy), as shown in Fig. 6(a–d). Notably, the highest occupied orbital, $1b_1$, of the T_2O molecule participates in the reaction and shows delocalization, whereas the three low-energy level orbitals, $3a_1$, $1b_2$ and $2a_1$, remain unchanged with little involvement in the reaction. In the doped systems, there is energy-level overlap among O and T atoms in T_2O at approximately ~−6, ~−9 and ~−21 eV, which illustrates

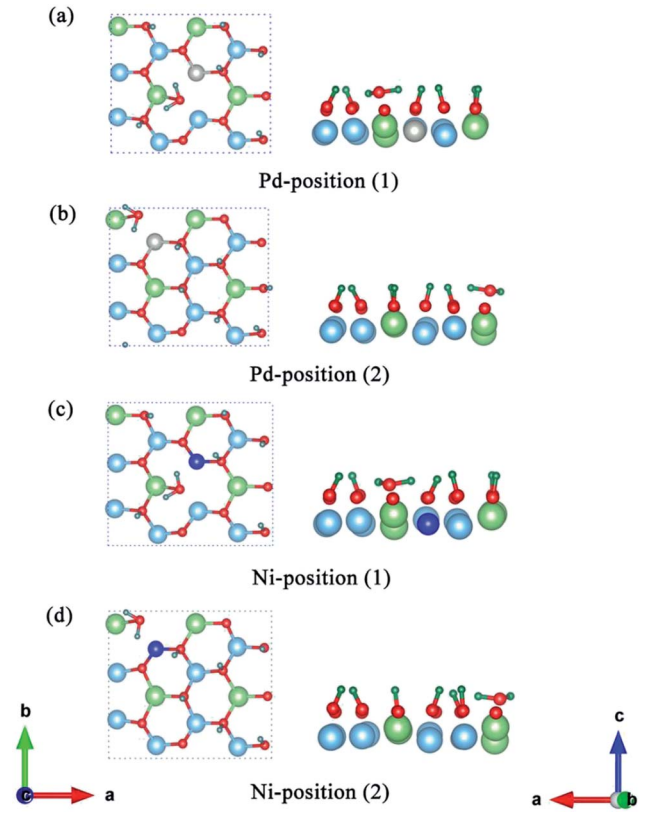

Fig. 5 Structure optimization of the Pd-T-Li_2TiO_3 surface (a and b) and Ni-T-Li_2TiO_3 surface (c and d). The left and right sides of each picture are the top and side views, respectively. The blue, green, red, silver, navy and dark green spheres represent Ti, Li, O, Pd, Ni and T atoms, respectively.

the formation of strong chemical bonds between O and T (T_1, T_2) atoms. Thus, the O orbital is partially filled with electrons from the orbits of the T_1 and T_2 atoms. A similar situation has been reported for report of H_2O adsorption on the surface of Li_4SiO_4.[37] In addition, there is no obvious hybridization between Li, Ti, and O or T atoms, which implies that the interaction is weak. In our calculations, the electrons injected into the O orbital may be from the T atoms; hence, O acts as an electron acceptor during the formation of T_2O on the DA-T-Li_2TiO_3 surface. Consequently, the interaction between O and T atoms closest to the doped atoms can be effectively enhanced by DA atoms. In the next section, we further confirmed this through Bader charge analysis on the DA-T-Li_2TiO_3 surface.

Table 5 Calculated O vacancy formation energy (in eV) for the pure and doped Li_2TiO_3 (001) surface

Surface	Site	O_{vac} formation energy (eV)
Pure-Li_2TiO_3		5.56
Pd-Li_2TiO_3	Position (1)	2.77
	Position (2)	2.74
Ni-Li_2TiO_3	Position (1)	3.51
	Position (2)	3.49

3.5 Bader charge analysis

Bader charge analysis (Table 6) revealed that charge transfer mainly occurs between the O atom and the two T atoms in the T_2O molecule. Specifically, O gains about 0.30 electrons and the two T atoms lose about 0.20 electrons respectively, on the Pd- and Ni-doped surface. This confirms the LDOS results from the previous section. However, there is greater transfer of electrons from Pd atoms than from Ni atoms. We speculate that the direction of and number of electrons transferred might depend on the specific element, which can be explained by differences in their electronegativity.[38] In general, an element with a higher electronegativity gains electrons from one with a lower electronegativity. The Pauling electronegativity of Pd is 2.20, which is larger than that of Ni (1.91).[39] This is the reason why Pd atoms gain more charge than Ni atoms from the surrounding atoms (Ti (1.54), T (2.20), O (3.34), Li (0.98)) in the Bader charge calculation. Combine with the previous study that the formation energy of the O vacancies in the Pd system is lower than that in the Ni system. Therefore, we speculate that Pd and Ni may affect the formation of O vacancies through charge transfer.

3.6 Charge density difference (CDD)

To further understand and analyze the interaction among T and O atoms on the surface of DA-T-Li_2TiO_3 (001), the CDD of the system was studied after T_2O formation. We defined the CDD as the difference between the charge density of the DA-T-Li_2TiO_3 system including T_2O molecules (C(DA-T-Li_2TiO_3, T_2O)), and the sum of the charge density of free T_2O molecule (C(T_2O)) and the DA-T-Li_2TiO_3 surface removing one T_2O molecule (C(DA-T-Li_2TiO_3)):

$$\mathrm{CDD} = C(\text{DA-T-Li}_2\text{TiO}_3, \text{T}_2\text{O}) - C(\text{T}_2\text{O}) - C(\text{DA-T-Li}_2\text{TiO}_3) \quad (4)$$

A real-space picture of the redistribution of the charge density upon T_2O formation is shown in Fig. 7.

After the formation of T_2O, there is a charge depletion region near the T atoms and a charge accumulation area near the O atom in the T_2O molecule on both doped surfaces. Electron transfer of Li and Ti can be ignored both in position (1) and (2) on the doped surfaces. There is slight charge transfer around the dopant atoms. This result is in agreement with the previous Bader charge analysis, which also means that the doped atoms can affect the bonding between O and T atoms and the formation of O vacancies through charge transfer.

3.7 Desorption of T_2O from Pd- and Ni-doped T-Li_2TiO_3 surfaces

The question addressed next is desorption of T_2O after its formation. T_2O will accumulate on the surface of T-Li_2TiO_3 if the T_2O cannot be discharged effectively from the device. This causes corrosion of the equipment, which, in turn, leads to metal poisoning and affects the catalysis of the dopant metal. Therefore, T_2O needs to be quickly desorbed from the Pd- and Ni-Li_2TiO_3 surfaces. The challenge is in overcoming the

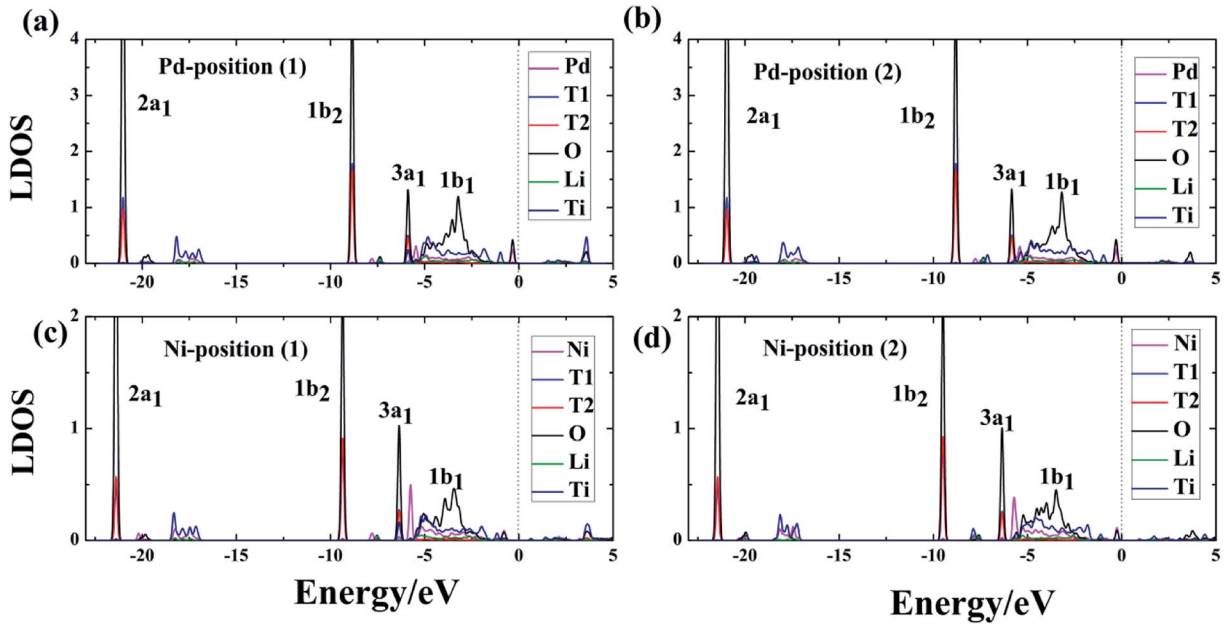

Fig. 6 (a)–(d) Local density of states (LDOS) for Pd- and Ni-doped T-Li_2TiO_3 surfaces. The blue, red and black curves represent the T_1, T_2 and O atoms of the T_2O in the surface. The olive, navy and magenta curves represent the LDOS for Li, Ti and DA, respectively. $1b_1$, $3a_1$, $1b_2$, and $2a_1$ represent four molecular orbitals of T_2O. The Fermi level is set to zero.

Table 6 Bader charge of T_2O and the T-Li_2TiO_3 (001) surface. ΔQ indicates the charge difference of atoms in the surface

Doping atoms (position)	ΔQ (e^-)					
	T_1	T_2	O	DA	Li	Ti
Pd (1)	−0.180	−0.240	0.360	0.133	−0.010	0.019
Pd (2)	−0.160	−0.210	0.310	0.137	0.006	0.018
Ni (1)	−0.120	−0.190	0.330	0.017	0.005	0.009
Ni (2)	−0.210	−0.190	0.320	0.017	0.002	0.008

desorption barrier of the T_2O (the calculated desorption energies are shown in Fig. 8). In this section, the pathways that minimize the desorption barrier are chosen based on the CI-NEB method. The final state was found by minimizing the energy of the T_2O molecule outside the slab.

In our analysis, T_2O is desorbed at a height of 3 Å on the surface. The corresponding potential barriers for concerted pathways are shown in Fig. 8, the desorption energies of T_2O molecules are ~0.30 and ~0.27 eV on the two positions of the Pd-T-Li_2TiO_3 surface, and ~0.48 and ~0.38 eV on the two positions of the Ni-T-Li_2TiO_3 surface. In contrast with the value of 1.956 eV for the Li_4SiO_4 surface,[36] the desorption energies of T_2O molecules in the doped systems are acceptable. The energy required for desorption varies greatly, which may be due to the different dopant atom. The similar calculations curve appears in the reports of the O_2 desorption from the carbon nanotube surface.[40]

In summary, based on our results and those of previous calculations, we conclude that the desorption energy is influenced by O vacancies. Moreover, because the desorption energies for the DA-T-Li_2TiO_3 surface are lower than those of the T-Li_2TiO_3 surface, it is evident that dopant atoms can reduce the energy for T_2O desorption. Finally, T_2O molecules can be effectively released under a lower energy barrier, and doping of the catalyst metal on the surface of Li_2TiO_3 can improve T release.

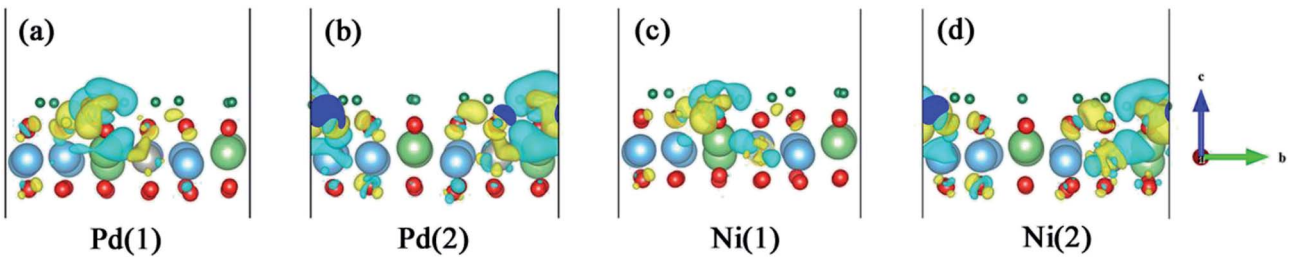

Fig. 7 Differential charge density obtained on the surface of DA-T-Li_2TiO_3, and (a and b) represent Pd-T-Li_2TiO_3 surface, (c and d) Ni-T-Li_2TiO_3 surface, respectively. The yellow region is the charge accumulation region and the blue-green region is the charge depletion region.

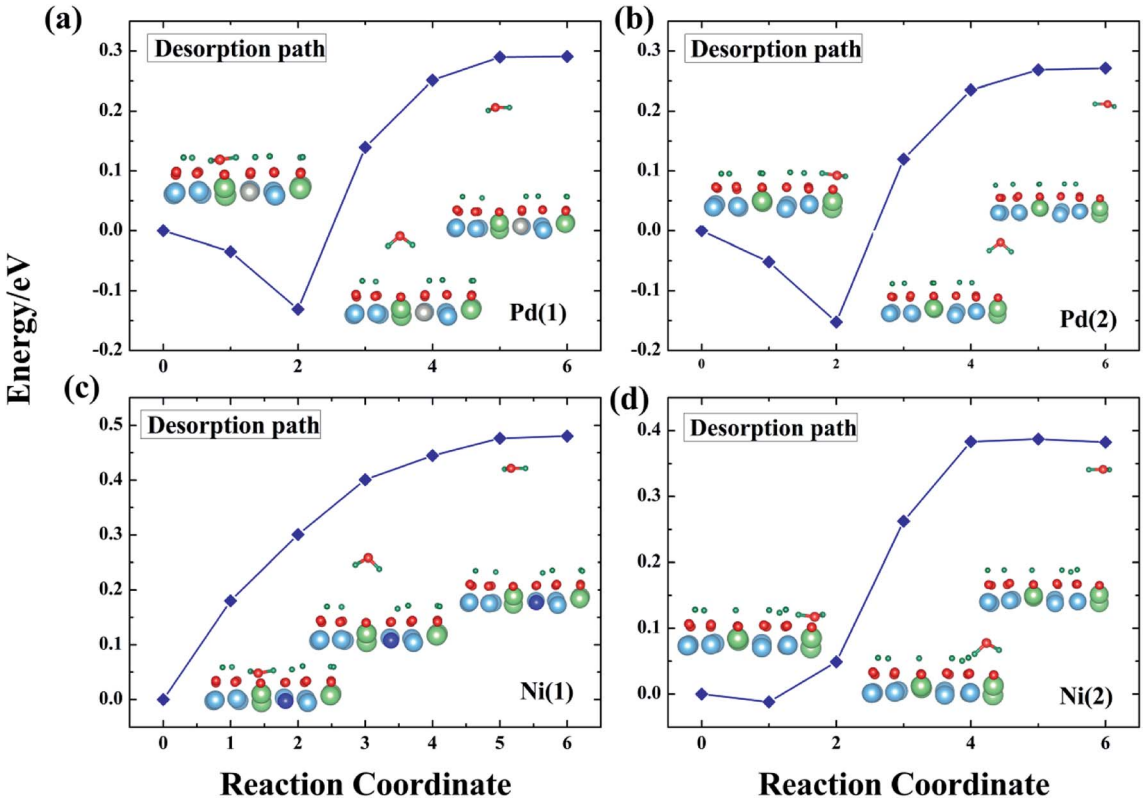

Fig. 8 T_2O desorption path for the Pd-T-Li_2TiO_3 surface (a and b) and the Ni-T-Li_2TiO_3 surface (c and d).

4. Conclusions

Our theoretical studies provide a clear account of the catalytic effect of Pd and Ni dopants on the release of T_2O molecule from the Li_2TiO_3 surface. The CI-NEB method revealed the formation and desorption energies of T_2O (0.94 and 0.64 eV, respectively) on the pure Li_2TiO_3 surface. Because the dopants reduce the formation energy of O vacancies on the DA-Li_2TiO_3 surface, T_2O generated spontaneously. Thus, metal catalysts can promote the desorption of T from the surface of Li_2TiO_3, which is consistent with previously reported experimental results.

To clarify the mechanism of the formation of T_2O molecules on the doped surface, we calculated the local density of state, Bader charge and charge density difference of the doped Li_2TiO_3 surface. We found that the OT group closest to the dopant atoms is affected by the dopants, which enhances the interaction with the adjacent T atoms during T_2O formation. O vacancies are more likely to be generated on the surface because of the dopant atoms, and O atoms in OT acquire electrons from T atoms. As a result, orbital hybridization occurs between O and T, and chemical bonds are formed. This leads to the spontaneous generation of T_2O molecules around the dopant atoms. The calculated desorption energy of T_2O molecules on the Li_2TiO_3 surface with metal catalysts was ~0.30 and ~0.48 eV in the Pd- and Ni-doped systems, respectively. Thus, the dopant atoms can reduce the energy for T_2O desorption. Taken together, our works demonstrates the potential of Pd and Ni as catalysts for the generation of T_2O and the release of T on the Li_2TiO_3 surface. We also hope that we can provide a better research direction for the release experiment.

Conflicts of interest

There are no conflicts to declare.

Acknowledgements

This work is supported by the ITER plan of the Ministry of Science and Technology of China (Grant No. 2014GB111001 and Grant No. 2014GB125002).

References

1 C. Johnson, *J. Nucl. Mater.*, 1999, **270**, 212–220.
2 C. E. Johnson, *J. Nucl. Mater.*, 1991, **179**, 42–46.
3 C. E. Johnson, *Ceram. Int.*, 1991, **17**, 253–258.
4 X. Kong, Y. Yu, S. Ma, T. Gao, C. Xiao and X. Chen, *RSC Adv.*, 2017, **7**, 35239–35250.
5 A. K. Fischer, *J. Nucl. Mater.*, 1992, **191**, 236–239.
6 X. Xiang, W. Zhu, T. Lu, T. Gao, Y. Shi, M. Yang, Y. Gong, X. Yu, L. Feng and Y. Wei, *AIP Adv.*, 2015, **5**, 107136.
7 D. Cruz, S. Bulbulian, E. Lima and H. Pfeiffer, *J. Solid State Chem.*, 2006, **179**, 909–916.
8 Y. Kawamura and M. Nishikawa, *J. Nucl. Mater.*, 1995, **218**, 57–65.

9 K. Noda, *Proceedings of the sixth international workshop on ceramic breeder blanket interactions*, Japan Atomic Energy Research Inst., 1998.
10 Y. Kawamura, K. Ochiai, T. Hoshino, K. Kondo, Y. Iwai, K. Kobayashi, M. Nakamichi, C. Konno, T. Yamanishi and T. Hayashi, *Fusion Eng. Des.*, 2012, **87**, 1253–1257.
11 T. Kinjyo, M. Nishikawa, M. Enoeda and S. Fukada, *Fusion Eng. Des.*, 2008, **83**, 580–587.
12 C. Johnson, K. Noda and N. Roux, *J. Nucl. Mater.*, 1998, **258**, 140–148.
13 M. Kobayashi, Y. Oya and K. Okuno, *J. Nucl. Mater.*, 2013, **439**, 159–167.
14 T. Kinjyo, M. Nishikawa and M. Enoeda, *J. Nucl. Mater.*, 2007, **367**, 1361–1365.
15 T. Tang and D. Luo, *Journal of Atomic and Molecular Sciences*, 2010, **1**, 185.
16 Y. Narisato, K. Munakata, A. Koga, Y. Yokoyama, T. Takata and H. Okabe, *J. Nucl. Mater.*, 2004, **329**, 1370–1373.
17 K. Munakata, A. Baba, T. Kawagoe, T. Takeishi, Y. Yokoyama, M. Nishikawa, R. D. Penzhorn, H. Moriyma, K. Kawamoto and K. Okuno, *Fusion Eng. Des.*, 2000, **49**, 621–628.
18 K. Munakata, Y. Yokoyama, A. Koga, N. Nakashima, S. Beloglazov, T. Takeishi, M. Nishikawa, R.-D. Penzhorn, K. Kawamoto and H. Moriyama, *J. Nucl. Mater.*, 2002, **307**, 1451–1455.
19 J. Kopasz, C. Seils and C. Johnson, *J. Nucl. Mater.*, 1992, **191**, 231–235.
20 P. E. Blöchl, *Phys. Rev. B: Condens. Matter Mater. Phys.*, 1994, **50**, 17953.
21 G. Kresse and D. Joubert, *Phys. Rev. B: Condens. Matter Mater. Phys.*, 1999, **59**, 1758.
22 G. Kresse and J. Furthmüller, *Phys. Rev. B: Condens. Matter Mater. Phys.*, 1996, **54**, 11169.
23 I. Mazin, D. J. Singh, M. Johannes and M.-H. Du, *Phys. Rev. Lett.*, 2008, **101**, 057003.
24 Y. Shi, *et al.*, *J. Nucl. Mater.*, 2015, **467**, 519–526.
25 H. J. Monkhorst and J. D. Pack, *Phys. Rev. B: Condens. Matter Mater. Phys.*, 1976, **13**, 5188.
26 G. Henkelman, B. P. Uberuaga and H. Jónsson, *J. Chem. Phys.*, 2000, **113**, 9901–9904.
27 Z. Wan, Y. Yu, H. Zhang, T. Gao, X. Chen and C. Xiao, *Eur. Phys. J. B*, 2012, **85**, 181.
28 J. , F. Dorrian and R. , E. Newnham, *Mater. Res. Bull.*, 1969, **4**(3), 179–183.
29 K. Kataoka, Y. Takahashi, N. Kijima, *et al.*, *Mater. Res. Bull.*, 2009, **44**(1), 168–172.
30 X. Xiao, F. Hayashi, K. Yubuta, A. Selloni and K. Teshima, *Cryst. Growth Des.*, 2017, **17**, 1118–1124.
31 N. Kuganathan, *et al.*, *Solid State Ionics*, 2018, **327**, 93–98.
32 Y. Zhang, *et al.*, *J. Nucl. Mater.*, 2017, **484**, 103–109.
33 T. Oda, H. Tanigawa and S. Tanaka, *Fusion Sci. Technol.*, 2003, **44**, 485–489.
34 G. Ran, C. Xiao, X. Chen, Y. Gong, C. Kang and X. Wang, *J. Nucl. Mater.*, 2015, **466**, 316–321.
35 Z. X. Yang, D. W. Ma, X. H. Yu, *et al.*, *Eur. Phys. J. B*, 2010, **77**(3), 373–380.
36 Z. Lu, Z. Yang, K. Hermansson, *et al.*, *J. Mater. Chem. A*, 2014, **2**(7), 2333–2345.
37 X. Kong, Y. Yu, S. Ma, T. Gao, C. Xiao and X. Chen, *Chem. Phys. Lett.*, 2018, **691**, 1–7.
38 D. Ma, W. Ju, T. Li, X. Zhang, C. He, B. Ma, Y. Tang, Z. Lu and Z. Yang, *Appl. Surf. Sci.*, 2016, **364**, 181–189.
39 A. Allred, *J. Inorg. Nucl. Chem.*, 1961, **17**, 215–221.
40 X. Y. Zhu, S. M. Lee, Y. H. Lee and T. Frauenheim, *Phys. Rev. Lett.*, 2000, **85**, 2757.